Journal of Applied Electrochemistry (2007) 37:63–70
DOI 10.1007/s10800-006-9210-3

Characterization of boron doped diamond during oxidation processes: Relationship between electronic structure and electrochemical activity

SIMONETTA PALMAS*, ANNA M. POLCARO, ANNALISA VACCA, MICHELE MASCIA and FRANCESCA FERRARA
Dipartimento di Ingegneria Chimica e Materiali, Università degli Studi di Cagliari, Piazza d'Armi, 09123, Cagliari, Italy
*(*author for correspondence, fax: +39-0706755067, e-mail: sipalmas@dicm.unica.it)*

Received 14 February 2006; accepted in revised form 24 April 2006

Key words: BDD electrode, catalytic activity, EIS technique, energetic band levels, flat band potential

Abstract

This work investigates the behaviour of BDD samples differently aged by an oxidative treatment. Two series of data are presented: the first in acid solutions was used to derive information about the electronic structure of the samples, whereas measurements in equimolar ferro/ferri cyanide solutions were performed to test the activity of the samples towards charge transfer reaction. Flat band potential as well as energy levels of conduction and valence bands were calculated for new and aged samples. These parameters, together with the current voltage response, are crucial information for a comprehensive interpretation of the behaviour of samples.

1. Introduction

The attention which boron doped diamond has attracted in this last decade is so great that citation of all the papers which have appeared in the literature is very difficult. Wide-ranging work has been carried out by several research groups, such as those of Swain [1–5], Fujishima [6–12], Comninellis [12–15] and Pleskov [16–19], just to cite some of their more recent papers. Some scientific journals and several congresses have been specifically devoted to the presentation of results obtained, both in basic studies and for possible applications of this material in electroanalytical devices and electrochemical processes [20–24]. Despite this, many questions are still open, especially as regards our understanding of the reaction mechanisms at the electrode surface, and the possible connections between catalytic activity and electronic structure of the sample [12, 25–29]. Among the different results which have been published, an objective comparison is complicated due to the lack of a standard diamond electrode material to compare results against. Several factors may influence the behaviour of different samples, such as doping type and level (i), morphological features (ii), non-diamond impurity content (iii), crystallographic orientation (iv), and surface group functionalities (v) [30]. Moreover, reproducible results can be achieved only if the past history of the electrode is known.

With this objective, an experimental study was started in our laboratory to investigate the effect of an oxidative process on the structure of a highly doped (HD) BDD sample. Some preliminary results have been submitted elsewhere [31]. The results from Raman analysis were combined with those from electrochemical investigation in order to justify the evolution of electrochemical activity and structural changes of BDD samples as the ageing time was increased. The results indicate that the behaviour of the samples may be explained by the displacement of H in the lattice: a considerable excess of H is actually added to stabilise B during film deposition.

On the basis of these results, the study was extended in this work to less doped samples (LD). The study was completed by an investigation of the capacitance–voltage characteristics that allowed calculation of the flat band potential and the energetic levels of conduction and valence bands of diamond, very important parameters in understanding the evolution of the sample behaviour with time.

2. Experimental section

Boron doped diamond (supplied by CSEM) with medium doping level (1300 ppm, 2.3 μM thickness) was used. The electrodes were assembled over a stainless steel base and electrical contacts were made with a silver-based paste to the back side of the substrate. The lateral faces were isolated with silicon wax. The surface working area was 1 cm^2 in all the experiments. The assembly was mounted as working electrode in a

conventional three electrode cell with SCE (saturated calomel electrode) as the reference electrode against which all the potential values in the text are referred. A large area platinum sheet was used as counter electrode. The electrodes were not pre-treated before the electrochemical ageing tests.

The cell was controlled by a potentiostat (Amel 7200), while the electrical impedance measurements were performed by a frequency response analyser (AMEL FRA 7050).

Ageing tests were performed in which the BDD samples were submitted to potentiostatic runs (E = 2.8 V) in 0.5 M sulphuric acid for about 10 h. At suitable intervals of time the tests were stopped and the samples were submitted to specific electrochemical investigation carried out both in direct current and in alternating current to evaluate their catalytic activity towards the redox couple ferro/ferri cyanide (0.5 M KNO_3; 5 mM $K_4Fe(CN)_6$; 5 mM $K_3Fe(CN)_6$).

Specific runs in sulphuric acid (0.5 M) were also carried out in order to get information on the electronic structure of the samples. In particular the MS (Mott-Shottky) analysis was performed through Electrochemical Impedance Spectroscopy measurements (EIS) carried out in a wide range of potential bias at which a sinusoidal signal with an excitation amplitude of 10 mV was superimposed. The impedance spectra were recorded in the frequency range 0.1 Hz–100 kHz. The resulting curves were fitted to suitable equivalent circuits by using the ZsimpWin software.

3. Results and discussion

In discussing the behaviour of BDD electrodes as the ageing time is increased, we start from the results obtained in previous work carried out at highly doped (HD) samples [31]. In that case, a wide variation in conductivity was measured as the working time was increased: the sample started from an initial state of very high conductivity, which tended to diminish rapidly during the first hour; then, a passivated state was achieved in which the lowest current was registered. As the working time increased, higher values of current were measured and the behaviour of the sample became semimetallic. The global trend was justified by the intrinsic movement of the H within the structure. In particular, the high initial conductivity was attributed to the excess of the weakly bonded H, while the involvement of the strongly bonded H was assumed to explain the observed increase in conductivity and the large enhancement of the oxidation rate of the reaction $Fe(CN_6)^{-3}/Fe(CN)_6^{-4}$. Raman measurements also confirmed the formation of new acceptor levels during the working period, as well as their decrease when the samples were left at rest for some time.

In the present work the research was extended: linear sweep voltammetry and impedance spectroscopy measurements were carried out at less doped samples (1300 ppm of B), aiming at improved characterization of the electronic structure of the samples to reveal a possible relation between semiconductor properties and kinetic behaviour in redox solution. Also in this case the outer-sphere redox reaction of ferro/ferri cyanide was used to test the activity of the surface towards the charge transfer, while specific runs carried out in sulphuric acid were devoted to obtaining information on the electronic structure of the samples.

3.1. *Runs in sulphuric acid – Mott-Shottky analysis*

The Mott-Shottky analysis is based on the assumption that in depletion conditions, the capacitance of the space charge layer is very low with respect to that associated with the diffusion layer, which may be, in turn, completely ignored.

In such conditions, it can be demonstrated that

$$\frac{1}{C_{SC}^2} = \frac{2}{q\varepsilon\varepsilon_0 N_a A^2}\left(|V - V_{fb}| - \frac{kT}{q}\right) \quad (1)$$

where C_{SC} = capacitance of the space charge layer; q = electron charge; ε = dielectric constant of diamond; ε_0 = permittivity of free space; A = area of the electrode; V applied bias potential; V_{fb} = flat band potential; N_a = acceptor concentration; k = Boltzman constant, and T = absolute temperature.

The reciprocal of the square of the capacitance per unit area gives a straight line when plotted as a function of the electrode potential: the acceptor concentration can be easily derived from the slope of the straight lines, while the flat band potential V_{fb} can be determined by extrapolation to $1/C^2 = 0$.

To obtain reliable data for MS analysis, impedance data for new and aged samples were obtained in the wide range of water stability window (Figure 1): the low faradic currents measured in this range provided favourable conditions for the measurement of the impedance diagrams. In fact, in the absence of appreciable faradic current, EIS measurements performed at potential lower than the flat band potential value can give useful information on the depletion layer charge distribution at p-semiconductors: in particular, just one semicircle should appear in the Nyquist diagram corresponding to the capacitive response of the space charge region [32].

Examination of the Nyquist plots shown in Figure 2 shows that the behaviour of the "as deposited" (AD) samples is quite different from the ideal: in a wide range of potential two semicircles are always present, even at potentials far from the flat band value.

The parameters of the equivalent circuits utilised to fit the experimental data (Table 1) indicate that the high frequency semicircle may be attributed to the response of a passivated layer since its capacitive term is scarcely influenced by potential [33]. Furthermore, the whole response of the electrode/solution interface may be correlated to the low frequency loop: as the potential is

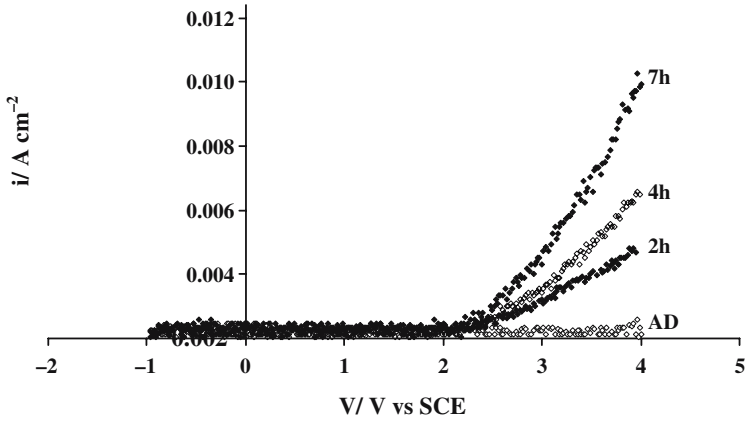

Fig. 1. Trend of linear sweep voltammetries (100 mV s^{-1}) in sulphuric acid at differently aged samples.

increased the capacitance component increases and, at the higher potential values, the effect of the capacity of the Helmoltz layer can also be included in the response. In such conditions, MS analysis is hardly applicable; indeed, difficulties in the application of this analysis at BDD electrodes are not infrequent [33–37]. In the vicinity of the flat band potential, the capacitance term is extremely sensitive to substrate polarisation due to change in the space charge within the semiconductor. Reliable data can only be obtained far from V_{fb}, so its value must be calculated by an extrapolation method. Following the suggestions of certain authors [32, 35], more reliable information can be obtained from the resistance component of the circuit, which, in depletion conditions, assumes very high values. The trend of $1/R$ with the potential can be effectively used: its value is almost zero in all the depletion region and suddenly rises to almost infinity when the potential approaches V_{fb}, which in turn can be evaluated without an extrapolation procedure. An example of $1/R$ vs V data for the AD sample is shown in Figure 3 from which the sharp variation of conductance is noticeable at about 1.2 V.

Table 1. Values of the fitting parameters evaluated from the equivalent (R(QR)(QR)) circuit at different potentials

Potential /V vs. SCE	Y_{01}/ μS s^n	n_1	R_1/Ω cm^2	Y_{02}/ μS s^n	n_2	R_2/ mΩ cm^2
0.4	0.23	0.88	461	11.02	0.93	5.76
0.8	0.22	0.89	461	12.20	0.92	0.97
1.2	0.23	0.88	452	13.65	0.92	0.35
1.4	0.21	0.89	449	21.22	0.85	0.03
1.8	0.22	0.89	458	38.41	0.76	0.012

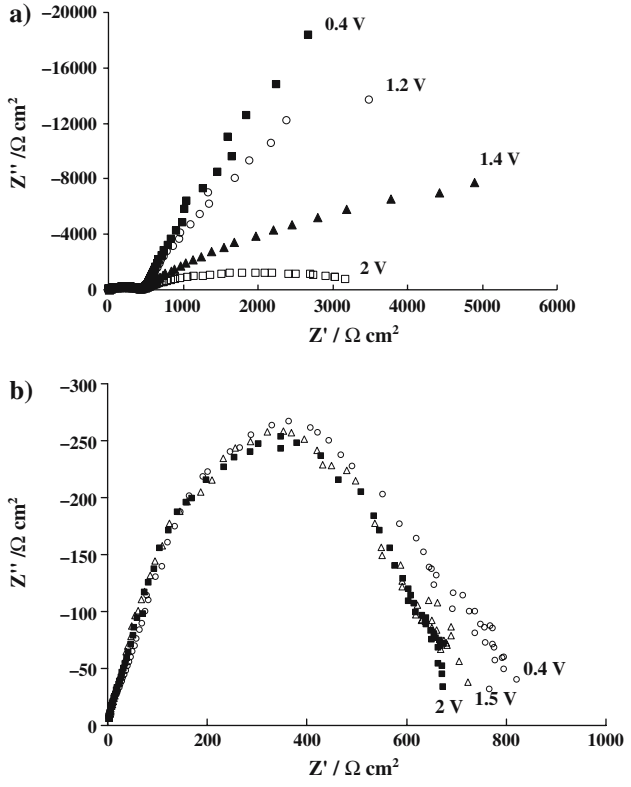

Fig. 2. Nyquist plot in sulphuric acid at AD (a) and aged (b) samples.

When aged samples are considered (Figure 2 b), the effect of the passive layer is less evident (the high frequency loop is absent) and a more linear trend of the MS plot is obtained. Figure 4(a and b) shows the trend of MS data calculated for aged LD and HD samples. As is often reported for semiconductor/electrolyte interfaces [37], in the present case frequency dependent capacitances are observed. Frequency dispersion may be due to a combination of factors such as surface roughness and dielectric relaxation phenomena in the depletion layer, which can give rise to a frequency dependent dielectric constant [38].

Table 2 shows the values of acceptor density and flat band potential calculated from the MS plot for HD and LD samples at different ageing times. The table also reports the energy levels of conduction and valence bands which were calculated by the following:

$$V_{BV} = V_{BP} + KT\ln\frac{N_a^{SC}}{N_{BV}} \qquad (2)$$

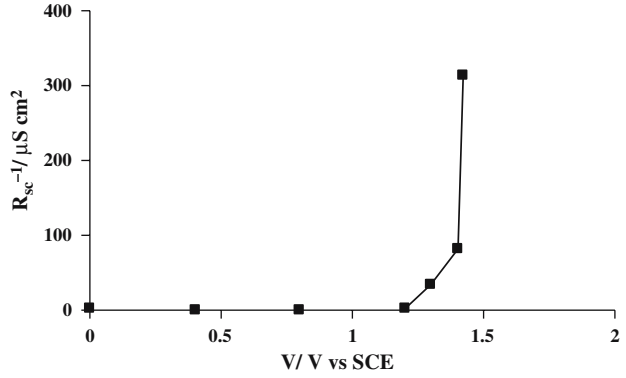

Fig. 3. Trend of the reciprocal of the depletion layer resistance for the flat band potential determination.

Table 2. Parameters deduced from the Mott-Shottky analysis for the different samples (subscripts indicate the ageing time)

Sample	Low doped		Highly doped	
	LD_{AD}	$LD_{7\ h}$	$HD_{2\ h}$	$HD_{350\ h}$
Flat band potential / V vs. SCE	1.2	1.8	1.3	2.5
Acceptor density / cm^{-3}	3.0×10^{18}	1.0×10^{19}	1.1×10^{19}	1.9×10^{19}
Conduction band / eV	−0.5	−1.2	−0.7	−1.6
Valence band / eV	−5.8	−6.5	−6.1	−7

where N_a represents the acceptor concentration in the space charge deduced from the MS plot, and N_{BV} is the effective density of the states in the valence band, which is a characteristic of the material (for diamond $N_{BV} = 10^{19}$ cm^{-3}).

As seen from data in Table 2, the oxidative treatment generates a shift in flat band potential to more positive values, as well as an increase in the concentration of the acceptors.

3.2. *Electrochemical activity – Runs in ferro/ferri cyanide*

3.2.1. *AD samples*

Figures 5(a and b) shows the Nyquist plots obtained in ferro/ferri cyanide solution at different potentials for AD samples. Full lines were obtained by fitting the experimental data to suitable equivalent circuits using ZsimpWin software (Table 3). One semicircle prevails up to a certain potential value, the global trend indicating a charge-transfer controlled process [39]. In fact, the low-frequency cut off on the real axis was found to decrease exponentially with potential, according to a Buttler Volmer trend. At potentials greater than 0.7 V, the trend is inverted: the intercepts of the circles increase with potential and a linear trend is registered in the lower frequency range, which may indicate mass transport control: a Warburg element W has to be inserted in the equivalent circuits to interpret data in this range of potential.

On the basis of the results obtained at HD samples, the observed behaviour can be justified by the lower doping level of LD samples examined in the present work: the lower excess of H, added in the structure to compensate B, determines the absence of the first state

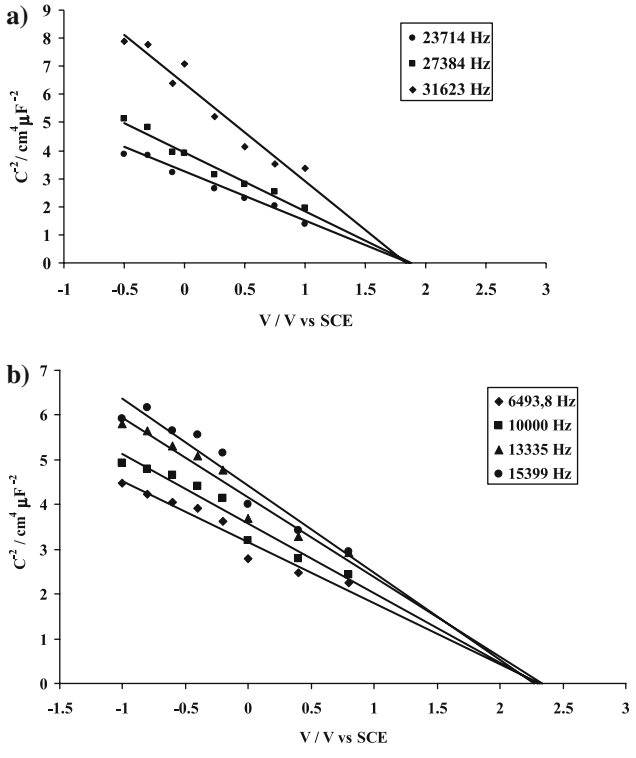

Fig. 4. Mott-Shottky plot obtained from AC impedance data at various frequencies, at LD (a) and HD (b) aged samples.

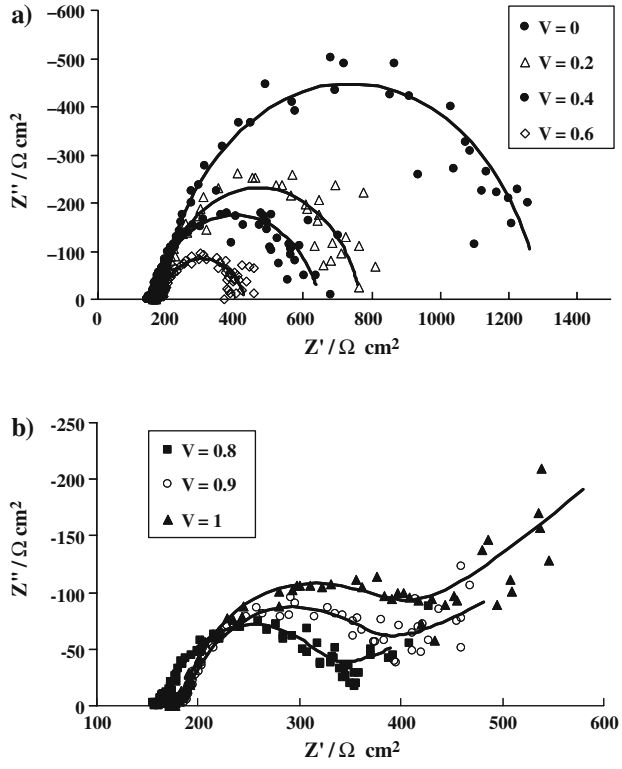

Fig. 5. Nyquist plot in ferro/ferri cyanide at AD sample at different potential bias. Full lines are calculated by fitting experimental data with equivalent circuits response.

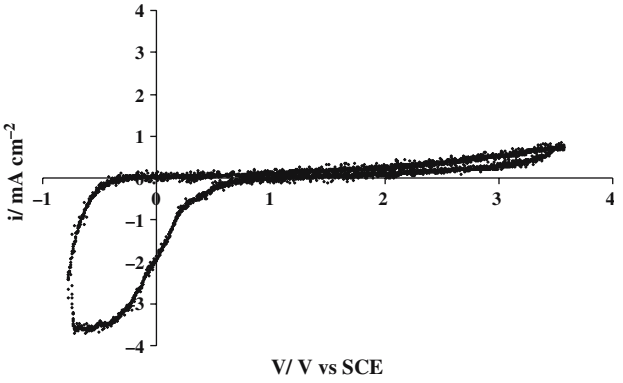

Fig. 6. Cyclic voltammetry at 100 mV s^{-1} in ferro/ferri cyanide at AD sample.

of initial high conductivity which was observed in HD samples. The AD sample should be in a passivated state, determined by a superficial layer where all B atoms are compensated by H. Thus, low current and high impedance values are registered at the surface.

To analyse the charge transfer activity of the different samples, data from voltammetric runs in ferro/ferri cyanide can also be considered. Particular attention has to be paid to the first voltammetric cycle registered at the AD sample (Figure 6): just a reduction peak was observed, while no signal of the corresponding peak was obtained in the oxidative scan, although the substrate is a p-type semiconductor. So on the basis of the Gerisher electronic model [40], the current density measured at the electrode surface of a semiconductor can be expressed as:

$$i^{-}(E) = -zF \int k(E) N_{\mathrm{o}}(E) D_{\mathrm{ox}}(E) dE \qquad (3)$$

where k is the transition coefficient, N_{o} is the number of occupied states in the conduction band, and D_{ox} is the number of vacant states due to oxidising species in solution. Naturally, a reciprocal expression will give the oxidation current i^{+}.

In our case, N_{o} is extremely low and should result in a vanishingly small cathodic current, a prediction which is in complete disagreement with results in Figure 6.

Other authors [41] have also underlined the unexpected absence of charge carrier supply limitations in reduction processes at BDD. In their case, having used solutions in which just the oxidised species was present, these authors justified the observed trend by assuming a direct involvement of the valence band of diamond in the charge exchange. In the present case, as specified above, a V_{fb} value of about 1.2 V was estimated, which leads to a position of the valence band at about −6 eV. Moreover, since the solution is equimolar in oxidised and reduced species, the Fermi level of the redox couple is surely higher than the valence band level, so a direct exchange of carriers has to be excluded; in any case, it could not explain the strong asymmetry between anodic and cathodic loops in the voltammetry.

Two different arguments can be used to justify the observed trend of current: on the one hand the formation

Table 3. Values of the fitting parameters evaluated from the equivalent circuit at different potentials at AD sample in ferro/ferri cyanide solution.

Potential /V vs. SCE	Equivalent circuit	Parameters			
		Y_0/S s^{n}	n	R /Ω cm^2	W /S $s^{0.5}$
0.1	R_s(QR)	$2.1. \times 10^{-5}$	0.83	900	–
0.2	R_s(QR)	2×10^{-5}	0.84	597	–
0.4	R_s(QR)	3.4×10^{-5}	0.78	499	–
0.6	R_s(QR)	4.1×10^{-5}	0.75	253	–
0.7	R_s(QR)W	2.9×10^{-5}	0.82	172	0.016
0.8	R_s(QR)W	2.9×10^{-5}	0.83	169	0.0054
0.9	R_s(QR)W	3.6×10^{-5}	0.80	200	0.003

of new superficial states originated by H which acts as donor

$$H \rightarrow H^+ + e^-$$

gives electrons which may be available for cathodic reaction. In this case, the current may be expressed by the Equation (3) which is modified by a term g_s, which represents the surface generation rate of the charge carriers. An analogous justification was given to explain the behaviour of p-silicon in reduction reactions [32].

On the other hand, depending on the applied potential, either the displacement of the superficial passivated layer within the bulk or its maintenance at the surface can be obtained [42], the two situations being strongly dependent on the charge of the H which is generated by the B:H complex reactions

$$B{:}H \rightarrow B^- + H^+$$

$$B{:}H \rightarrow B^- + H^0 + h^+$$

In the specific case, during the cathodic scan the H present in the structure as H^+ should drift in the electric field, thus being swept out of the depletion layer, and finally recaptured at the end of the space charge region by an unpassivated boron acceptor. As a consequence, the boron acceptors in the depletion layer will be reactivated and the passivated layer will be shifted deeper into the bulk. This may explain why the application of a reducing potential, although reverse biasing for a p-type semiconductor, leads to local reactivation of the surface with consequent increase in current, whereas an oxidative potential, which should be direct biasing, tends to maintain the H^+ in the passivated layer and to limit the observed anodic current.

3.2.2. *Aged samples*

As the working time increases, a net increase in anodic current is measured. At the same time, as observed from Figure 7, the impedance registered in the EIS measurements falls and the diffusive regime is achieved at a potential lower than that for the AD sample. Moreover, analogously to what was observed for HD samples [31], cyclic voltammograms in ferro/ferri cyanide are more regular and the oxidative peak appears in the loop, indicating a more activated surface; the peaks are more symmetrical (Figure 8), although still widely separated, indicating that reversibility of charge transfer is not yet achieved.

Analysis of the electronic structure of the sample is useful in determining the factors that play a major role in the observed behaviour. As reported above, one of the main effects of ageing is the increase in acceptor concentration, which in turn leads to an increase in current (Equation (3)). However, the shift of the valence band towards energetic values far from the Fermi level of the solution suggests that the valence band is not directly involved in the charge exchange, so new states, caused by superficial defects or changes in the grain boundaries of the polycrystalline diamond film, could be responsible for the observed metallic-like character.

This argument is supported by the EIS measurements obtained at aged samples which were left at rest for some months. A new capacitive element is observed in the Nyquist diagram (Figure 9), which was attributed to the capacitive response of the grain boundaries at which poly-acetylene terminations originated during the ageing tests. Due to the high ratio R_{ct}/R_F between charge transfer and film resistances, the capacitive response of the film was not visible in the previous spectra, which were registered before the rest period of the samples.

Analogous behaviour observed at more doped samples [31] was justified by considering that after a sufficiently long period of time, the H concentration gradient, originating during the previous working period, was partially compensated by a slow diffusive process of H from bulk to surface. This caused a decrease in conductivity due to the partial re-compensation of B atoms and the consequent decrease in the free acceptor levels. Thus, the increased value of film resistance allows its capacitive response to be revealed.

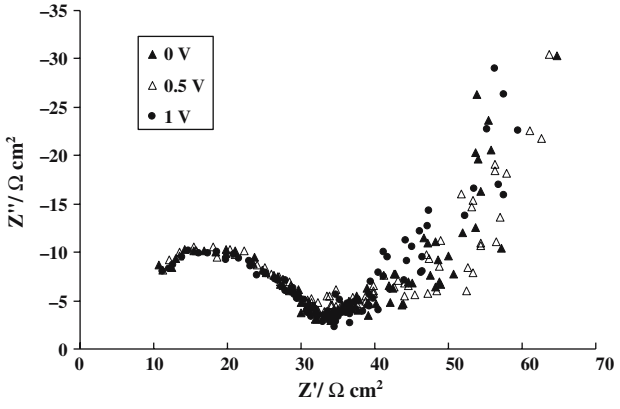

Fig. 7. Nyquist plot in ferro/ferri cyanide at aged sample at different potential bias.

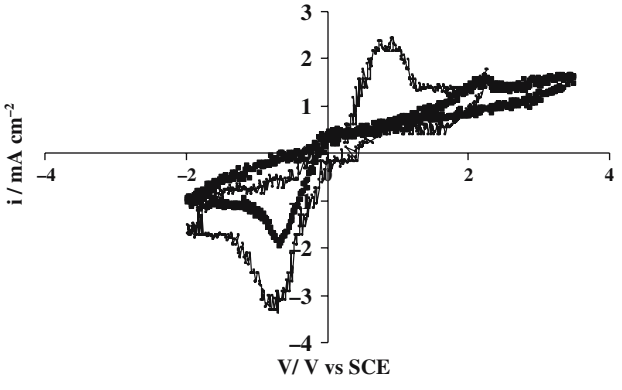

Fig. 8. Cyclic voltammetries (100 mV s^{-1}) at aged (2 h and 7 h) samples in ferro/ferri cyanide solutions.

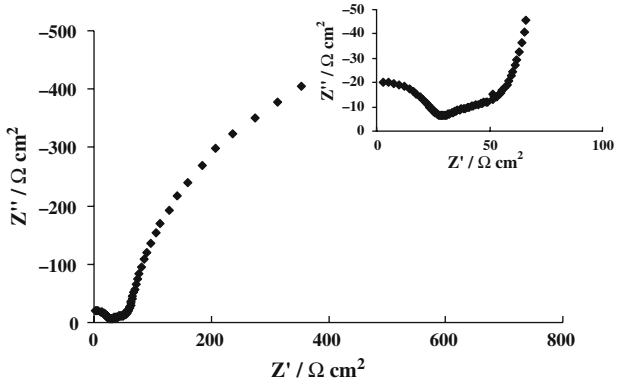

Fig. 9. Nyquist plot in ferro/ferri cyanide at an aged sample which was left at rest for 1 month.

4. Conclusions

The results obtained at medium doped BDD show that the behaviour of the sample is similar to that observed at more doped samples. The most significant differences may be related to the lower conductivity of the less doped samples. Because of the lower doping level, the excess of H added to the structure to compensate B is lower. This determines the absence of the first state of initial high conductivity which was observed in highly doped samples. The AD sample should be in a passive state determined by a superficial layer where all B atoms are compensated by H. Thus, low current and high impedance values are registered at the surface.

However, this situation tends to be rapidly modified and, as the working time is increased, the samples tend to be more conductive.

Analysis of the electronic structure indicates that the main effect of the oxidative ageing is a shift of the flat band potential to more positive potentials which, in turn, determines a shift of the energy levels of the bands towards more negative values. This excludes direct involvement of the valence band in the charge transfer process.

As was verified at more doped samples, the generation of new superficial states can be reasonably assumed to justify the increased metallic behaviour of the samples.

References

1. K.B. Holt, A.J. Bard, Y. Show and G.M. Swain, *J. Phys. Chem. B.* **108** (2004) 15117.
2. A.E. Fischer and G.M. Swain, *J. Electrochem. Soc.* **152** (2005) B369.
3. G.W. Muna, V. Quaiserova-Mocko and G.M. Swain, *Anal. Chem.* **77** (2005) 6542.
4. G.W. Muna, N. Tasheva and G.M. Swain, *Environ. Sci. Technol.* **38** (2004) 3674.
5. K.L. Soh, W.P. Kang, J.L. Davidson, S. Basu, Y.M. Wong, D.E. Cliffel, A.B. Bonds and G.M. Swain, *Diamond Rel. Mater.* **13** (2004) 2009.
6. J. Wang, G. Chen, M.P Chatrathi, A. Fujishima, D.A. Tryk and D. Shin, *Anal. Chem.* **75** (2003) 935.
7. C. Terashima, T.N. Rao, B.V. Sarada, D.A. Tryk and A. Fujishima, *Anal. Chem.* **74** (2002) 895.
8. C. Terashima, T.N. Rao, B.V. Sarada, Y. Kubota A. Fujishima, *Anal. Chem.* **75** (2005) 1564.
9. K. Honda, Y. Yamaguchi, Y. Yamanaka, M. Yoshimatsu, Y. Fukuda and A. Fujishima, *Electrochim. Acta* **51** (2005) 588.
10. T. Kondo, K. Honda, D.A. Tryk and A. Fujishima, *J. Electrochem. Soc.* **152** (2005) E18.
11. A. Manivannan, N. Spataru, K. Arihara and A. Fujishima, *Electrochem. Solid-State Letts.* **8** (2005) C138.
12. I. Duo, C. Levy-Clement, A. Fujishima and Ch. Comninellis, *J. Appl. Electrochem.* **34** (2004) 935.
13. G. Siné and Ch. Comninellis, *Electrochim. Acta* **50** (2005) 2249.
14. E. Mahé, D. Devilliers and Ch. Comninellis, *Electrochim. Acta* **50** (2005) 2263.
15. L. Ouattara, M.M. Chowdhry and Ch. Comninellis, *New Diamond Frontier Carbon Technol.* **14** (2004) 239.
16. Yu. V. Pleskov, Yu. E. Evstefeeva, M.D. Krotova, P.Y. Lim, S.S. Chu, V.G. Ral'chenko, I.I. Vlasov, (...), H.C. Shi, Russ. J. Electrochem. **41** (2005) 337.
17. Yu V. Pleskov, Yu E. Evstefeeva, V.P. Varnin and I.G. Teremetskaya, *Russ. J. Electrochem* **40** (2004) 886.
18. Yu V. Pleskov, Yu E. Evstefeeva, M.D. Krotova, V. Ya Mishuk, V.A. Laptev, Yu.N. Palyanov and Yu M. Borzdov, *J. Electrochem. Soc.* **149** (2002) E260.
19. Yu V. Pleskov, M.D. Krotova, Yu E. Evstefeeva, V.G. Ral'chenko, I.I. Vlasov and A.V. Khomich, *Russ. J. Electrochem* **37** (2001) 1123.
20. N. Bensalah, A. Gadri, P. Canizares, C. Saez, J. Lobato and M.A. Rodrigo, *Environ. Sci. Technol.* **39** (2005) 7234.
21. X. Chen, G. Chen, F. Gao and P.L. Yue, *Environ. Sci. Technol.* **37** (2003) 5021.
22. C.A. Martínez-Huitle, S. Ferro and A. De Battisti, *J. Appl. Electrochem.* **35** (2005) 1087.
23. A.M. Polcaro, A. Vacca, S. Palmas and M. Mascia, *J. Appl. Electrochem.* **33** (2003) 885.
24. M.A. Rodrigo, P.A. Michaud, I. Duo, M. Panizza, G. Cerisola and Ch. Comninellis, *J. Electrochem. Soc.* **148** (2001) D60.
25. D. Becker and K. Juttner, *Electrochim. Acta* **49** (2003) 29.
26. N.G. Ferreira, L.L.G. Silva, E.J. Corat and V.J. Trava-Airoldi, *Diamond Rel. Mater.* **11** (2002) 1523.
27. D.A. Tryk, K. Tsunozaki, T.N. Rao and A. Fujishima, *Diamond Rel. Mater.* **10** (2001) 1804.
28. R. Ramesham, *Thin Solid Films* **315** (1998) 222.
29. R. Ramesham, *Sensors Actuators B* **50** (1998) 131.
30. I. Duo, A. Fujishima and Ch. Comninellis, *Electrochem. Comm.* **5** (2003) 695.
31. A.M Polcaro, P.C. Ricci, S. Palmas, F. Ferrara and C. Anedda, Thin Solid films, (in press), doi: 10.1016/itsf.2006.06.033.
32. M. Chemla, J.F. Dufreche, I. Darolles, F. Rouelle, D. Devilliers, S. Petitdidier and D. Levy, *Electrochim. Acta* **51** (2005) 665.
33. T. Kondo, K. Honda, D.A. Tryk and A. Fujishima, *Electrochim. Acta* **48** (2003) 2739.

34. Yu V. Pleskov, V.M. Mazin, Yu E. Evstefeeva, V.P. Varnin, I.G Teremetskaya and V.A. Laptev, *Electrochem. Solid-State Letts.* **3** (2000) 141.
35. V. Bretagna, R. Erre, F. Rouelle, M. Chemla, S. Petitdidier and D. Levy, *Electrochim. Acta* **47** (2001) 129.
36. G. Pastor-Moreno and D.J. Riley, *Electrochim. Acta* **47** (2002) 2589.
37. J. van de Lagemaat, D. Vanmaekelbergh and J.J. Kelly, *J. Electroanal. Chem.* **475** (1999) 139.
38. W.P.F Gomes Cardon, *Progr. Surf. Sci.* **12** (1982) 155.
39. Liu Meilin and Wu Zhonglin, *Solid State Ionics* **107** (1998) 105.
40. H. Gerisher, *Electrochim. Acta* **35** (1990) 1677.
41. A.D. Modestov, Yu E. Evstefeeva, Yu V. Pleskov, V.M. Mazin, V.P Varnin and I.G. Teremetskaya, *J. Electroanal. Chem.* **421** (1997) 211.
42. R. Zeisel, C.E. Nebel and M. Stuzmann, *Diamond Rel. Mater.* **9** (2000) 413.